

Evaluating the role of product gas composition in vibrational relaxation in pulsed microwave plasma-enhanced flames

Fynn Reinbacher*, Sarang Bidwai[†], James B. Michael[‡]
Department of Mechanical Engineering, Iowa State University, Ames, Iowa, 50011

Ryan J. Thompson[§] and Chloe E. Dedic[¶]
Department of Mechanical and Aerospace Engineering, University of Virginia, Charlottesville, Virginia, 22904

Hybrid fs/ps coherent anti-Stokes Raman scattering (CARS) is employed to investigate the vibrational temperature evolution of N_2 in lean methane flames exposed to pulsed microwave irradiation. Vibrational temperature during and post microwave illumination by a 2 μ s, 30 kW peak power, 3.05 GHz pulse is monitored in flames diluted with N_2 , N_2 and CO_2 , and N_2 and Ar. Electric field strengths inside the microwave cavity are monitored directly using electric field probes. Temperature increases up to 140 K were observed in flames with additional Ar and CO_2 dilution, whereas temperature increases by 80 K were observed in mixtures diluted with only N_2 . The microwave energy deposition to excited states begins to thermalize over scales of $100~\mu$ s, however, equilibrium is not reached before excited combustion products convect out of the probe volume on the order of several 1~ms. Understanding the impact of varying bath gases on microwave interaction, magnitude of temperature rise and thermalization timescales is critical for the development and validation of new kinetic models for applications exhibiting significant degrees of thermal non-equilibrium, such as high-speed reentry flows and plasma-assisted combustion.

I. Introduction

Lame enhancement in plasma-assisted combustion is the thermo-physical response of the combustion system to the creation of a thermal non-equilibrium by an external electric field, and the subsequent relaxation (thermalization) of the excited degrees of freedom [1]. The degree of non-equilibrium induced by an applied field can result in excitation of additional energy in translational, rotational, and vibrational degrees of freedom. In addition, increased dissociation and ionization can be prevalent. The specific degree of non-equilibrium depends on both the available electron energy and species present in the reactive system. In laminar premixed flames, enhancement from applied sub-critical continuous microwave (MW) fields has shown an increase in laminar flame speed [2–4]. In addition, higher field strength (above breakdown threshold) pulsed microwave application has been shown to extend the lean extinction limit of ignition kernels [5]. Multiple pathways and mechanisms have been proposed for microwave flame interactions including reaction pathways sensitive to ionization, and ohmic heating [3, 6]. Investigating the role of non-equilibrium effects and mechanisms, however, remains a challenge. While vibrational energy transfer rates and ionization kinetics have received much attention in the field of high-speed aerodynamics, coupling plasma and combustion kinetic models remains challenging and requires further studies of vibrational-vibrational (V-V) and vibrational-translational (V-T) transfer processes [7–10].

Coherent anti-Stokes Raman scattering can be used to measure rotational and vibrational energy distributions simultaneously [11–13] and has been used in a variety of studies in combustion and non-equilibrium environments [14–19]. Due to the high spatial and temporal resolution that can be achieved with hybrid fs/ps CARS the method lends itself in particular to study environments such as laminar flames exposed to pulsed microwave illumination as demonstrated by Dedic and Michael [20, 21]. In their study of methane-air flames, they observed little initial vibrational excitation during the MW pulse, followed by an additional increase of vibrational temperature post MW illumination. Vibrational excitation occurred on the timescale of V-V transfer processes, however, the lack of further evidence of

^{*}Graduate Research Assistant, Student Member.

[†]Graduate Research Assistant, Student Member.

[‡]Associate Professor, Member.

[§]Graduate Research Assistant, Student Member

[¶]Assistant Professor, Member.

vibrational states with v > 2 suggests that quenching of excited electronic states and recombination may be important. Similarly, the subsequent thermalization occurred over timescales much longer than expected based on V-T relaxation rates [22] for species in the reaction products. For the multicomponent products typical in air-breathing combustion systems, investigations of the impact of different gas species are necessary to elucidate the contributions to thermalization rates in plasma-enhanced flames.

In shock tube experiments it has been observed that even small fractions of argon in N₂ and CO can increase the vibrational relaxation time significantly [23–25]. Cutler et al. [12] investigated the flow at the University of Virginia Supersonic Combustion Facility using CARS to verify the impact of water vapor vibrational non-equilibrium in nitrogen and oxygen. In dry gas mixtures, large degrees of vibrational non-equilibrium were present in both N₂ and O₂, while rotational temperatures were thermally equilibrated. While any steam addition caused O₂ to attain thermal equilibrium, some non-equilibrium with remained in N₂ at lower steam fractions. Similar effects have been noted in the supersonic tunnels with plasma excitation in the upstream plenum, where the addition of CO₂ promoted faster thermalization [26]. Tiwari et al. [27] investigated the stability of DC no-transferred arc plasma jets via emission spectroscopy and high-speed imaging and noted noticeably different behaviors in Ar, N₂ and Air plasmas. Differences in defining behaviors between simulations and experiments occur in flows where relaxation timescales compete with reaction timescales. As such, the detonation cell size of H₂ detonations differs between simulations and experiments, under conditions where the vibrational relaxation time of H₂ is on the same timescale as the ignition delay time [28].

In the current work, the impact of product gas composition on pulsed microwave interaction with laminar flames was investigated. Lean methane-oxygen flames were examined with varying dilutions consisting of nitrogen, nitrogen and argon, and nitrogen and carbon dioxide. Hybrid fs/ps CARS was used to measure the time evolution of vibrational N₂ temperatures in the product gases following pulsed microwave illumination. In order to more accurately quantify reduced electric field strengths, coaxial probes were employed in similar configuration to Nilsson et al. [29]. These measurements will allow for comparisons in thermalization timescales with a range of collisional partners in the product gas composition.

II. Theory and Experimental Methods

A. Hybrid fs/ps CARS Theory and Experimental Setup

Hybrid fs/ps coherent anti-Stokes Raman scattering is generated in a medium through a nonlinear, four-wave mixing process. It is an interaction of three distinct laser pulses within a media. Two of the pulses are temporally short and spectrally broad, namely the pump (ω_1) and Stokes (ω_2) beams. These pulses are intended to excite the rotational/vibrational Raman transitions of the molecules. In hybrid fs/ps CARS the third pulse, referred to as the probe (ω_3) beam, is spectrally narrow and temporally long [30, 31]. In this study, the probe beam will be frequency narrowed using a second harmonic bandwidth compressor (SHBC) which will generate a 2.9 cm⁻¹ beam.

To simulate the CARS signal, a time-domain CARS model is simulated by capturing the time-dependent Raman response. The molecular Raman response, which is proportional to the CARS intensity field can be written as [32, 33]:

$$R(t) = c \sum_{i \ f} (\frac{\partial \sigma}{\partial i} \Delta \rho) e^{-(i\omega_{i,f} + \Gamma_{i,f})t}, \qquad (1)$$

where $\frac{\partial \sigma}{\partial}$ is the Raman cross-section, $\Delta \rho$ the population difference, $\omega_{i,f}$ the frequency of the state transition between states i and f, and $\Gamma_{i,f}$ the collisional finewidth. The CARS polarization can be simplified to [34?]:

where E_i refers to the complex electric field envelope of the three corresponding laser pulses, * denotes the complex conjugate, and $\tau_{2,3}$ refers to the delay between probe and Stokes beams.

A schematic of the hybrid fs/ps CARS setup is shown in Fig 1(a). A regeneratively amplified Ti:sapphire laser (Coherent Astrella F), centered at 800 nm is used to directly produce the Stokes beam. The probe beam is generated via a second harmonic bandwidth compressor (SHBC), which produces a 2.9 cm^{-1} , 400 nm beam [35]. The pump beam for vibrational CARS (VCARS) is generated using frequency doubled output of an optical parametric amplifier (OPA). It is centered around 674 nm for N_2 vibrational thermometry. A motorized delay stage allows precise control of the probe delay ($\tau_{2,3}$). All three beams are focused to the volume of interest using a 300 mm focal length plano-concave

lens using a BOXCARS phase-matching configuration.	The signal is dispersed using a 0.303 m Spectrometer (Andor

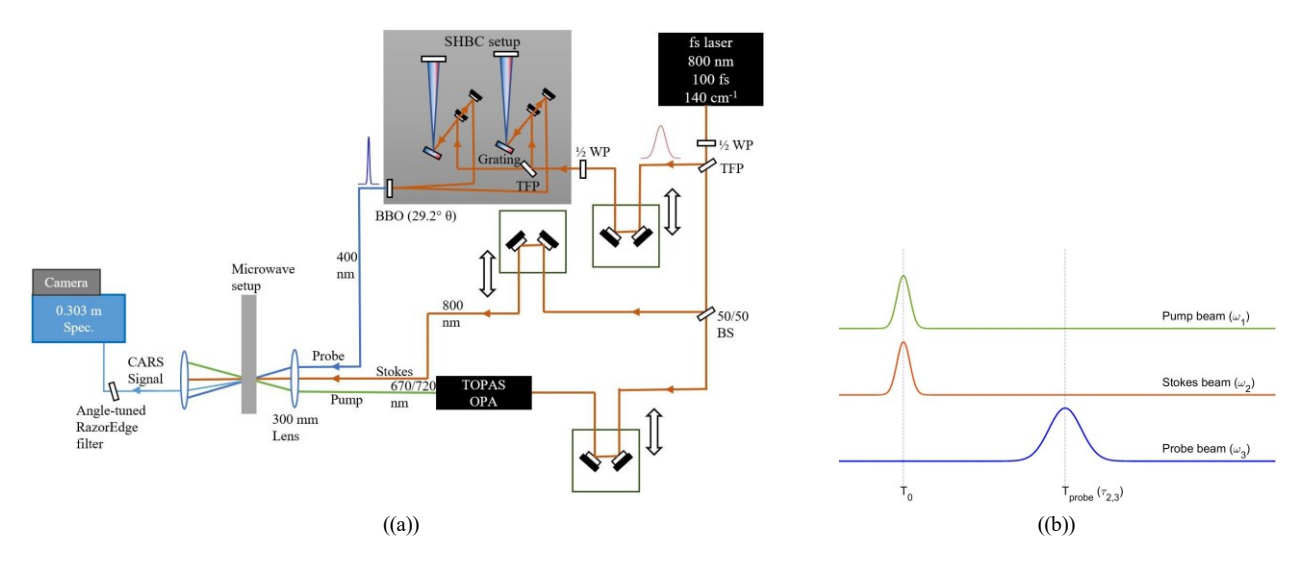


Fig. 1 a) Schematic of hybrid fs/ps CARS setup for vibrational CARS (VCARS) thermometry. Abbrs: WP = waveplate, BBO = Beta Barium Borate crystal, OPA = optical parametric amplifier, TFP = thin film polarizer, BS = beam splitter. b) Timing of the pump, Stokes, probe pulses

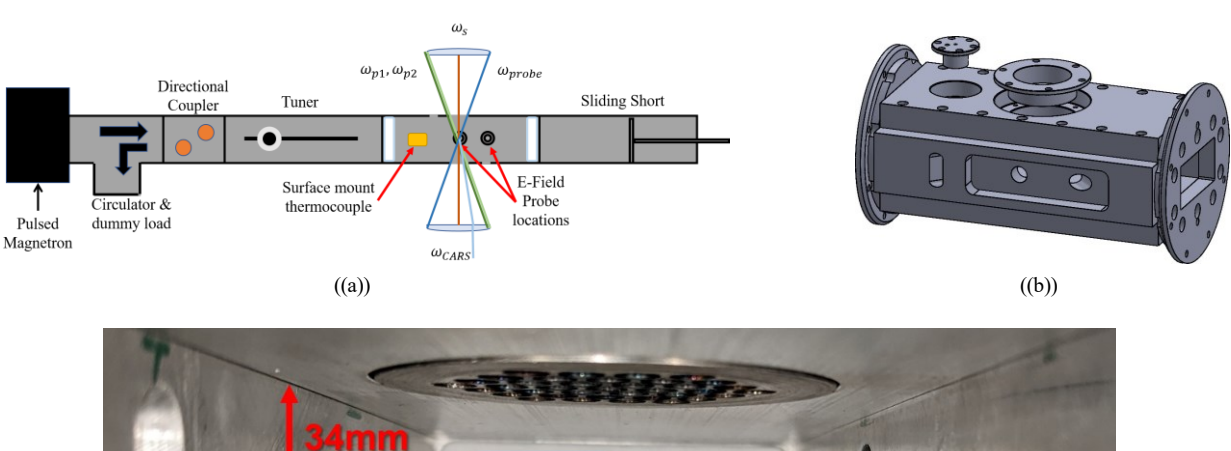
Shamrock SR-303i) and collected using an EMCCD camera (Andor Newton DU-970). Validation of CARS temperature measurements was performed using a hydrogen-air adiabatic Hencken burner flame [32]. Averaged N₂ CARS signal from the Hencken flame and a non-resonant background scan in Ar was used to verify pulse parameters:speccifically, the probe delay, frequency chirp parameters of probe pulse, and wavelength calibration of the spectrometer. These parameters were then used to build a library of CARS spectra as a function of temperature. Averaged CARS signal from the flat flame burner inside MW cavity was then fit for temperature across the library using a differential evolution algorithm [36].

B. Microwave Flame Experimental Setup

A resonant microwave cavity with an S-band magnetron (New Japan Radio M1302A) is used to create the pulsed microwave field with 30 kW peak power in a frequency range between 3.04 GHz and 3.06 GHz. Square wave pulses approximately 2 μ s in length, generated by a pulse generator (Pulse Systems Inc.), were used to drive the magnetron at a pulse repetition rate of 10 Hz. Precise timing between microwave pulses and the CARS beams was controlled using a digital delay generator (Stanford Research Systems DG545). The cavity consists of WR284 wave guide sections, including a circulator with a water-cooled dummy load, a -60 dB directional coupler, a sliding screw tuner, a custom aluminum test section for the burner, and a sliding short. Figure 2 shows a schematic of the microwave cavity setup and custom WR284 waveguide test section. Adjustment of the sliding short allowed for positioning of the E-field node at the desired location within the cavity test section. The sliding screw tuner was subsequently used to optimize the impedance matching within the waveguide. The guided wavelength of the TE₁₀ mode at 3.05 GHz in the cavity is $\lambda_g = 13.44$ cm.

1. Custom WR284 Test Section

The custom WR284 waveguide test section features three access ports in the side walls for optical and probe beam access through one angled circular 0.5 in hole, one angled 1 in tall, 0.25 in wide slit, and one 0.82 in tall, 0.5 in wide slit at the center. Paths of all three ports intersect at the cavity center at 45° and 90° . Two cutouts in the flat side of the cavity section (figure 2(c) top) can be used to add additional elements to the test section. The center cutout can be completed alternatively with either an E-field probe or carbon steel screen insert to allow hot combustion products to escape the cavity and therefore limit heating of the cavity and condensation of water vapor. Additionally, two 0.5 in thick PTFE windows were press-fitted into the end flanges of the waveguide section to prevent water vapor or any reactants from spreading and building up in the cavity prior to ignition. The second cutout allows for the addition of an E-field probe at $0.5\lambda_g$ from the center. A custom flange connection fitted to the bottom of the test section was used to mount a flat flame (McKenna) burner flush to the bottom of the cavity.



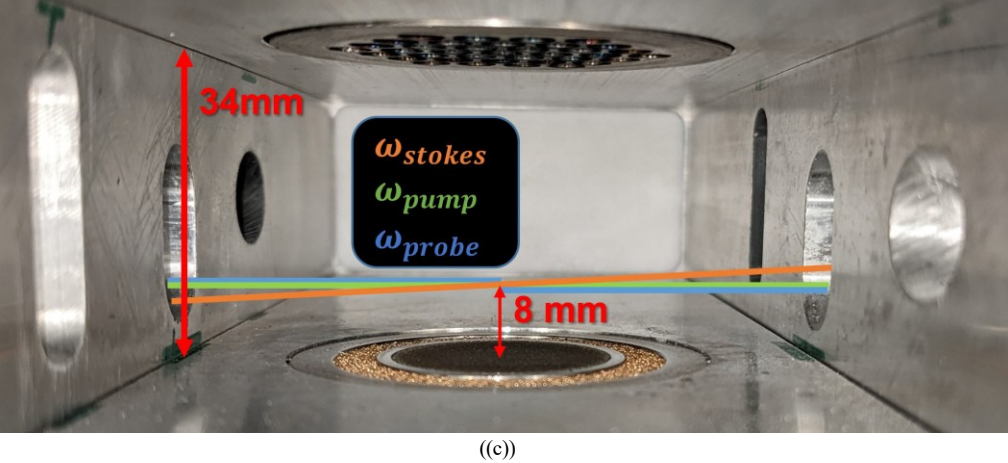


Fig. 2 a) Schematic of pulsed microwave cavity configuration, CARS beam geometry, and the E-field probe location. b) Rendering of custom WR284 test section. Variable inserts allow for the addition of flush-mounted electric field probes at the center of the waveguide section and a $\lambda_g/2$ offset. Cutouts in sides allow for imaging and probe beam access at 45° and 90° intersections. c) Interval view of cavity cross-section. The CARS probe volume was located 8 mm above the center of the burner surface.

2. E-Field Probes

The E-field probes are based on a design by Burkart [37] and were previously employed by Nilsson et al. [29] in the study of laminar flames exposed to microwave radiation. The advantage of this configuration is that it allows for direct and continuous measurement of the E-field strength throughout the course of the experiment. In comparison, previous studies had to rely on prior measurements of cavity quality or modeling. According to Burkhart [37] the electric field strength can be obtained from a power measurement of the coaxial probe. Power and electric field strength are related by

$$P = \frac{Z_0}{2} \left[\omega \epsilon_0 E_r K \right]^2. \tag{3}$$

Here Z_0 is the 50 Ω impedance of the coaxial probe, ω the microwave frequency, ϵ_0 the dielectric constant, and K is a constant, dependent on the probe geometry. In this experiment, the field probes were made from semi-rigid 0.085 in

coax cable (Amphenol RF 135101-R1). The cable was cut and secured with set screws in the cavity probe inserts so that the cable protruded approximately 0.5 mm. It was then ground flush with the surface and polished. A network analyzer (Anritsu MS46322A) was used to determine the coupling efficiencies, which were found to be -71.0 dB and -71.3 dB for center and side probe respectively. E-Field probe power measurements were made during experiments using calibrated Schottky rectifier diodes (Pasternack PE8003) and a digital oscilloscope (Picoscope 4824, 20 MHz bandwidth).

3. Flat Flame Burner

A flat flame was generated using a porous-plug flat flame burner (Holthuis and Associates). The burner consists of 25 mm diameter, water-cooled, sintered bronze burner plug, and sintered bronze shroud ring. Premixed fuel, oxidizer, and diluent mixtures flow through the center plug at a combined flow rate of 5 slpm, surrounded by an argon shroud. Three different lean fuel, oxidizer, and diluent mixtures were under investigation. Lean methane-air with an equivalence ratio of $\phi = 0.70$ was used as a reference mixture. To investigate the impact of Ar and CO₂, mixtures of one part N₂ and one part Ar and CO₂ were added. The total dilution fraction was adjusted to maintain approximately the same adiabatic flame temperature at a constant equivalence ratio. Table 1 shows the equilibrium mole fractions and adiabatic flame temperatures of the test mixtures used in this study, obtained using Cantera [38] and the GRI-MECH 3.0 reaction mechanism [39]. A nitrogen mole fraction of at least 30% was necessary in order to obtain a sufficient CARS signal.

Diluent	φ	X_{N2}	X_{Ar}	X_{CO2}	X_{O2}	X_{H2O}	$T_{ad}(K)$
N ₂ (Air)	0.70	73.4%	0%	6.9%	5.6%	13.7%	1846
$N_2 - Ar$	0.70	38.4%	38.4%	6.0%	7.1%	11.9%	1859
$N_2 - CO_2$	0.70	33.6%	0%	42.1%	5.0%	16.8%	1859

Table 1 Equilibrium mole fractions and adiabatic flame temperatures of selected test gas mixtures.

III. Results

A. Theoretical Impact of MW radiation

Electron energy loss coefficients for different excitation modes, weighted by mole fractions of the respective species are shown in Figure 3. Loss coefficients were calculated using Bolsig+ [40], for the product mixtures listed in Table 1. Electron scattering cross sections were obtained from the LX-Cat database[41–45]. Dashes and dotted vertical lines mark reduced field strengths corresponding to electric field strengths at the center of the cavity, measured by the electric field probes shown in Figure 4. The dashed line at 120 Td corresponds to the field strength measured in the tuned, empty cavity. Each dotted line marks the residual field strength at the center of the cavity with flame, at the beginning, after the initial drop of the electric field strength, and end of the microwave pulse. For N₂ they indicate the range 74 Td to 110 Td, for N₂ and Ar the range 60 to 87 Td, and for N₂ and CO₂ the range 80 to 100 Td.

In all three mixtures it can be seen that two of the primary energy loss mechanisms result from interactions with nitrogen molecules, specifically N₂ vibrational and electronic excitation, shown by the solid and dot-dashed blue lines. In the relevant reduced field strength range, the next highest energy loss fractions common among all three mixtures are, electronic excitation of H₂O, O₂ impact dissociation, and CO₂ electronic excitation (yellow solid, orange dotted, and purple dot-dashed lines). For mixtures with additional CO₂ dilution, i.e. 34% N₂ and 42% CO₂ in the products, in Figure 3(c), CO₂ electronic excitation occurs at a similar magnitude to N₂, as well as CO₂ vibrational excitation. At reduced field strengths of the order of 100 Td and greater, additionally CO₂ ionization starts to occur at similar magnitude to the mostly vibrational and electronic excitation modes. In mixtures containing argon, Figure 3(b), compared to those containing only N₂ as a diluent, Figure 3(a), the relative roles of N₂, CO₂, O₂, and H₂O remain constant. The main difference is the additional electronic excitation of argon, and ionization of argon for reduced field strengths greater than 100 Td.

Figure 3(d) shows the combined loss of all species to different excitation modes including vibration, electronic, impact dissociation, and ionization, for the three different diluent cases. In direct comparison, the highest degree of direct vibrational excitation across all species can be expected in gas mixtures with only nitrogen as a diluent. Mixtures containing a larger fraction of CO₂ or Ar will however experience higher degrees of initial electronic excitation, impact dissociation, and ionization. An increase in ionization in particular would be expected to impact additional microwave interaction, due to an increased amount of free electrons. Additionally, different vibrationally excited species such as CO₂, CO, O₂ and N₂ will have different vibrational relaxation times [46]. In shock tube experiments it has been observed that even small fractions of argon in N₂ and CO can increase the vibrational relaxation time significantly [23–25].

Figure 4 shows the inferred electric field strength at the center of the microwave cavity above the flat flame burner through the measurement of field strength at a $\lambda_g/2$ offset. Each trace pictured is averaged from 32 individual microwave pulses. Little pulse-to-pulse variation was observed with a variation of less than 1%. The drop in electric field strength is indicative of microwave absorption by the flame. Total absorption in flames diluted with N_2 , and N_2/CO_2 are similar in magnitude. More initial absorption of microwaves can be observed in case of the N_2/CO_2 mixture up to $t=0.5~\mu s$, whereas the absorption in plain N_2 diluted flames is slightly higher at later times in the microwave pulse. Overall higher absorption is observed in N_2/A r diluted flame.

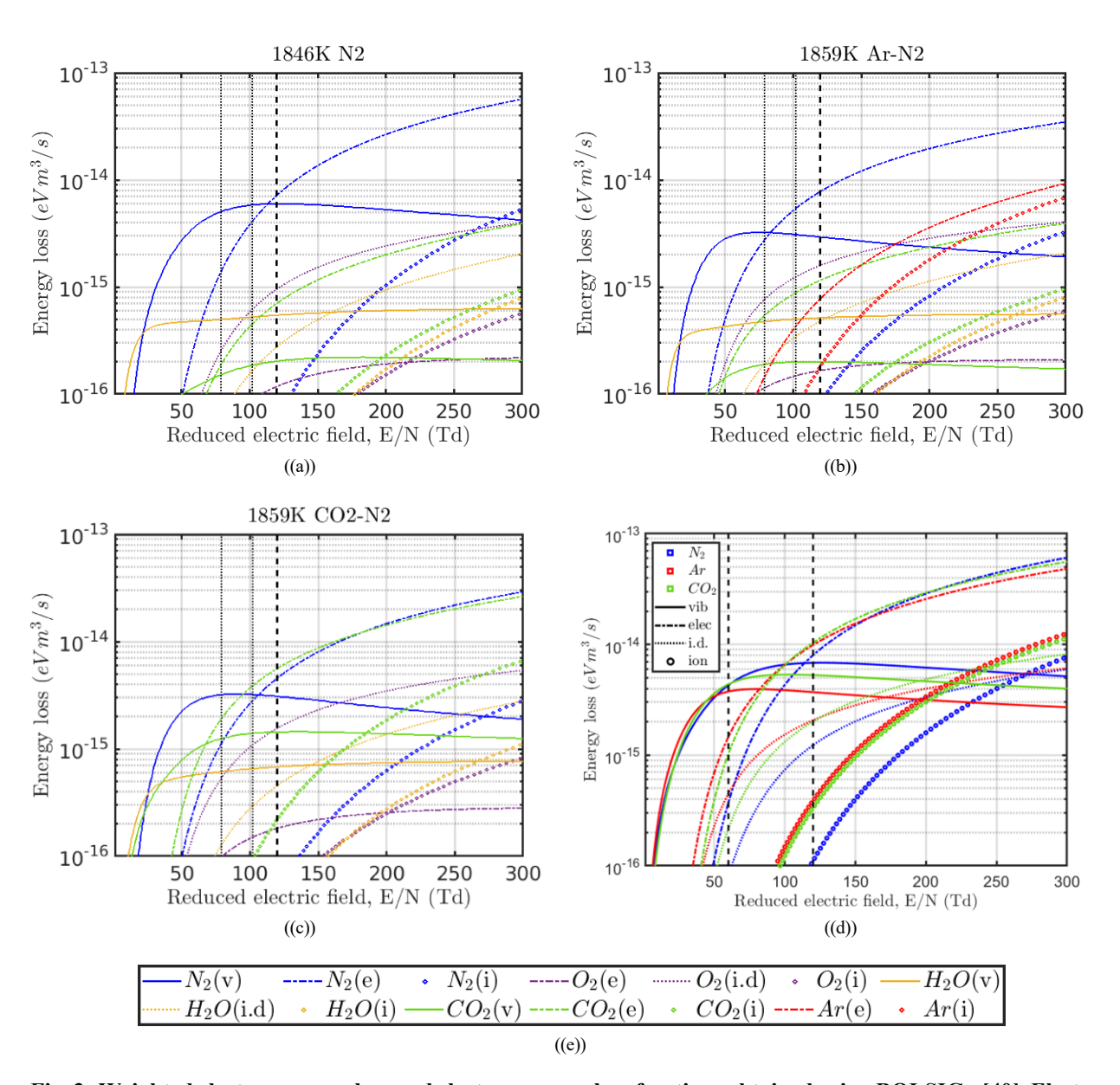


Fig. 3 Weighted electron energy loss and electron energy loss fractions obtained using BOLSIG+ [40]. Electron energy loss weighted by mole fraction at adiabatic flame conditions at 1850 K (table 1). a) Diluted with N₂, b) diluted with N₂ and Ar, c) diluted with N₂ and CO₂, d) comparison of total loss to different modes. Depicted are electron energy loss fractions for various species and modes of excitation. (v) vibrational excitation, (e) electronic excitation, (i) ionization, and (i.d.) impact dissociation.

B. CARS Thermometry Results

CARS spectra for N₂ vibrational temperature measurements were collected at varying delays with respect to the beginning of the microwave pulse. Time delays were varied from -1 µs to 90 ms. For flames diluted with plain N₂, 1000 individual spectra were collected at each time delay. Due to the reduced number density of nitrogen in mixtures containing additional CO₂ or Arin the diluent, on-sensor accumulation of CARS signal was used to improve SNR. For CO₂/N₂ diluted mixtures, signal from 3 instances was collected for each individual spectrum, for Ar/N₂ diluted mixtures signal from 5 pulses. In each mixed diluent case, 500 spectra were collected per pulse delay time. Regardless, the SNR in these accumulated single-shot measurements was insufficient to allow for single-shot fitting and temperature measurements at this time. Spectra were averaged to allow for temperature fitting. Even post accumulation and averaging

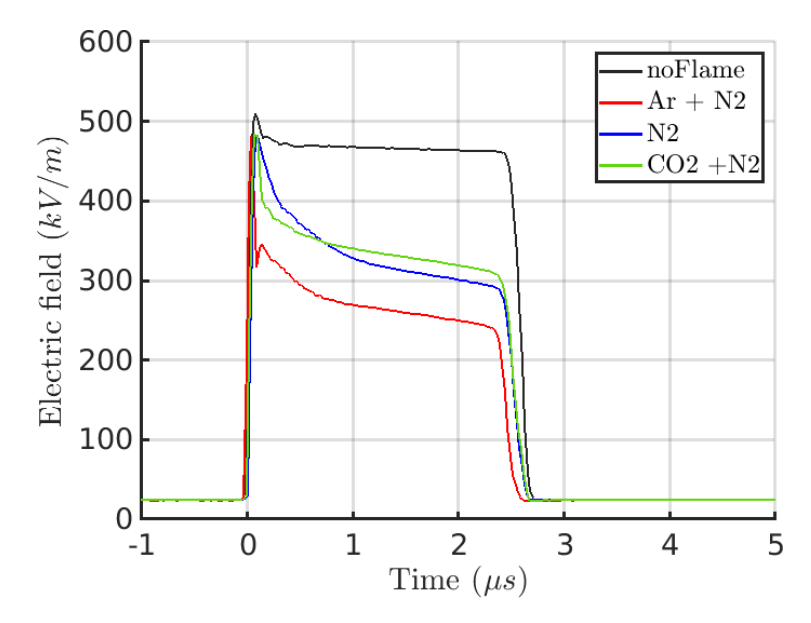


Fig. 4 Electric field strength at cavity center above burner, without flame and with flame with different inert gas diluents.

of 2500 individual CARS signal in 5(b), the fit quality did not match that of the average of 1000 individual probe signals in 5(a).

Shown in Figure 5 are averaged experimental and best-fit CARS spectra of microwave illuminated, N_2 and Ar/N_2 diluted flames at time delays varying from 0 μ s to 50.01 ms. The two main peaks are at about equal height at 0 μ s delay, before any interaction between microwave and flame as occurred. At the end of the microwave pulse around 2 μ s the peak height ratio shifts and the center peak is higher than the right most peak. This difference reaches a maximum around 10 μ s. After several ms the system relaxes back to its original state and the two main features are at equal height after 50 ms.

Shown in Figure 6 are the temperature changes relative to the average temperature measured in the flame without microwave illumination. Data taken at delays of $-1~\mu s$ and 0 μs are displayed at 0.09 μs and 0.1 μs respectively. Additional data was taken between delays of 1 ms and 10 ms, however, they exhibited signs of additional laser microwave-plasma interaction [47]. In this timescale, one or multiple laser pulses with 1 kHz repetition rate would either interact with the plasma around the time of microwave illumination or with the still excited plasma during the relaxation process. Some values in this timescale range were therefore omitted from Figure 6 at this point.

The vibrational temperature of nitrogen starts to increase above the flame temperature throughout the period of microwave illumination, which ends at approx. 2 μ s. In the pure N₂ dilution case the temperature increase at t=2 μ s is approximately 30 K. In cases with additional Ar and CO₂ dilution the initial temperature rise during the microwave illumination is significantly larger, 75 K in the case of Ar addition and 110 K in the case of the CO₂ addition, compared to 30 K in N₂ only dilution. In all three gas mixtures, the peak vibrational N₂ temperature is reached around 6 μ s after the beginning of the microwave illumination, or roughly 4 μ s after the end of the microwave illumination. The peak temperature reached in the case of pure N₂ dilution at approximately 80 K, is significantly lower than peak temperatures reached in mixtures with Ar and CO₂, which both peak around 140 K. In all three cases some initial relaxation and decrease in T_{vib}^{N2} can be observed between the peak at t=6 μ s and 10 μ s, and it continues to decrease until t=100 μ s. Up until about 1 ms the N₂ vibrational temperature at the measurement location appears to remain nearly constant until it starts to decay back towards the equilibrium flame temperature t=50 ms.

Temperatures before the microwave pulse and at time delays larger than 50 ms after the microwave pulse are approximately the same as in the flame without microwave illumination. This indicates that no interaction between subsequent pulses occurs, which would cause an increase in equilibrium flame temperature or baseline shift. At a combined flow rate of 5 slpm of the reactants, the maximum flow velocity in the flame products can be estimated to be between 0.25 m s^{-1} and 1 m s^{-1} . A flow speed of 1 m s representing the flow of equilibrium reaction products through a stream tube the diameter of burners center bronze plug. The entirety of the gas in the CARS probe volume, 8 mm

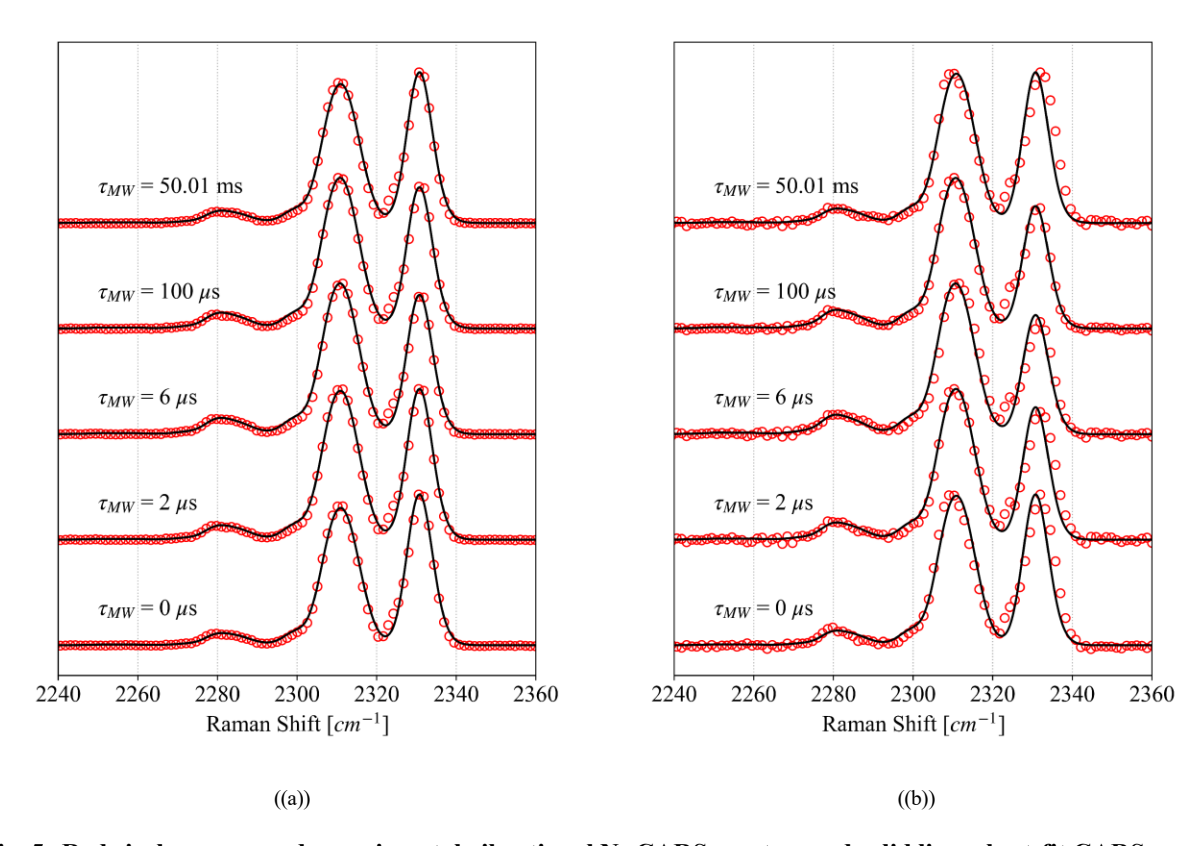


Fig. 5 Red circles: averaged experimental vibrational N_2 CARS spectra, and solid lines: best-fit CARS spectra in N_2 (a) and $Ar+N_2$ (b) diluted flames at various time delays with respect to the onset of the microwave pulse. Each shown spectrum in (a) is the average of 1000 single-shot measurements. Each spectrum shown in (b) is the average of 500 on-camera accumulations of 5 individual CARS measurements.

above the burner surface, should therefore be replaced with fresh combustion products not previously exposed to the microwaves within 8 to 32 ms. This convective timescale corresponds roughly to the timescale of the delays at which a decline of the vibrational N_2 temperature can be observed. Lower temperature differences at 10 μ s and later can therefore not be directly associated with relaxation or thermalization processes.

As indicated by Figure 3, the dominant initial inelastic electron collisional processes in all three gas mixtures are electronic excitation, vibrational excitation, ionization of N_2 , CO_2 and Ar, and impact dissociation of O_2 . The initial increase in vibrational temperature during the microwave pulse up to 2 μ s in all three cases can be attributed to direct excitation of vibrational modes by the microwave radiation. Additional microwave-induced ionization in flames with additional Ar and CO_2 likely causes the larger increase compared to flames with plain N_2 dilution. Relaxation of electronically excited modes (either directly excited or excited through collisional or recombination processes) over the next few μ s likely causes the additional increase in T_{vib} between 2 μ s and 6 μ s.

While increased variations in temperature in mixtures with Ar addition correlate with increased microwave absorption, as seen in Figure 4, flames with additional CO₂ dilution show a similar increase in excitation, while microwave absorption is not increased and on par with that in flames with N₂ dilution only.

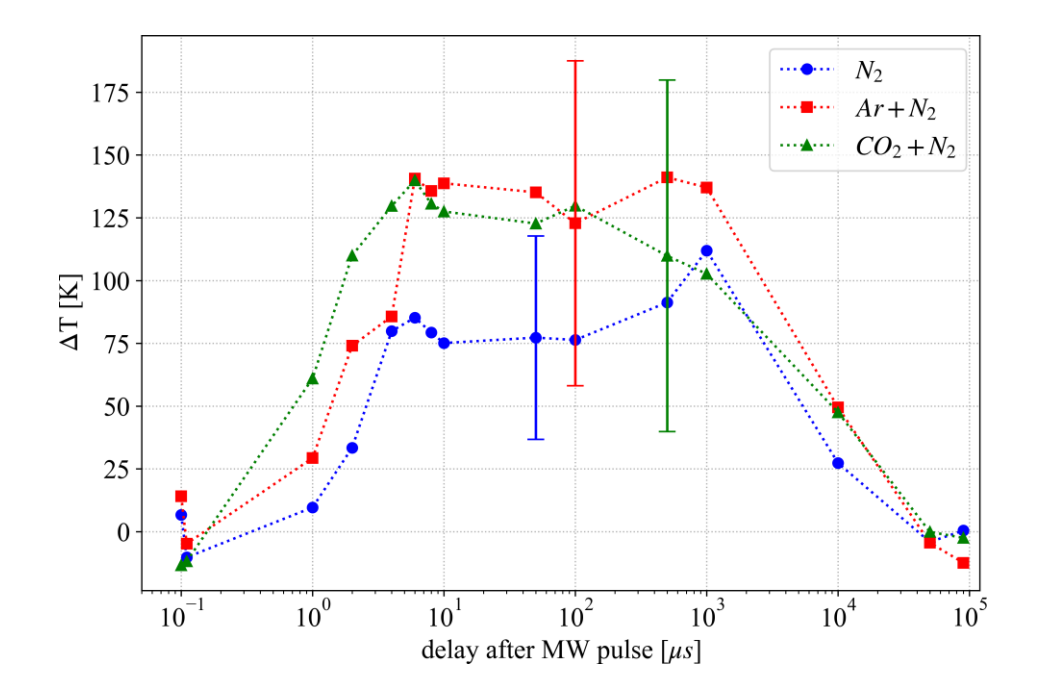


Fig. 6 Change in vibrational N_2 temperature obtained from averaged CARS spectra as a function of delay time with respect to the beginning of the microwave pulse. $\Delta T=0$ is defined by the temperature measured in the flame without microwave illumination. Data points displayed at $t=0.09~\mu s$ and $t=0.1~\mu s$ were measured at delays of

 $-1 \mu s$ and $0 \mu s$ respectively.

IV. Conclusion

The interaction of pulsed microwave radiation with lean methane flames and the impact of the flame diluent composition were investigated while holding the adiabatic flame temperature and density fixed. Vibrational N₂ temperatures at different time delays with respect to the microwave pulse were measured via hybrid fs/ps CARS spectroscopy, while electric field strengths were monitored via an electric field probe, and relevant electron energy loss mechanisms were investigated from solutions of the Boltzmann equations obtained using BOLSIG+ [40]. Field strengths between 60 Td and 120 Td were measured, which vary during each microwave pulse as absorption into the microwave-driven flame plasma increases. A significant increase in maximum vibrational temperatures of N₂ was observed in mixtures containing 38% N₂ and Ar, and 34% N₂ and 42% CO₂ at equilibrium flame conditions, when compared to flames with similar adiabatic flame temperature containing primarily N₂ (73%) as a diluent. Both Ar and CO₂ provide additional pathways for ionization and electronic excitation, likely adding to increased microwave interaction. The Ar addition resulted in increased vibrational excitation of N₂ after microwave exposure along with increased microwave energy absorption, while CO₂ addition resulted in a similar increase in excitation without any additional absorption.

These results highlight the important role the bath gas composition plays in microwave flame interactions, and the need for further investigation. Not resolved in this current study were vibrational temperatures at timescales between 1 ms and 10 ms due to laser microwave interactions, and therefore any potential thermalization processes that took place before gas was exposed to the microwaves in the CARS test volume was replaced by fresh combustion products. Future efforts will aim to resolve this issue as well as improve the signal to noise ratio, in order to obtain single-shot measurements and observe any shot-to-shot variations similar to what was reported in [21]. Additionally, the recent efforts by Thompson and Dedic for CO₂ thermometry [48] will allow a fuller range of gas compositions while monitoring additional species for the dynamics of relaxation following the application of microwave pulses. Measurements of populations in excited vibrational and electronic states of multiple combustion-relevant species will provide valuable insight and data critical to the validation of plasma and combustion kinetic mechanisms.

Acknowledgments

This material is based upon work supported by the National Science Foundation under Grant No. 1839551. Additional instrumentation support was provided by ONR through Grant No. N000142012838 and AFOSR through Grant No. FA9550-15-1-0195. Any opinions, findings, and conclusions or recommendations expressed in this material are those of the author(s) and do not necessarily reflect the views of the National Science Foundation or the Federal Government.

References

- [1] Starikovskiy, A., and Aleksandrov, N., "Plasma-assisted ignition and combustion," *Progress in Energy and Combustion Science*, Vol. 39, No. 1, 2013, pp. 61–110.
- [2] Jaggers, H., and Von Engel, A., "The effect of electric fields on the burning velocity of various flames," *Combustion and Flame*, Vol. 16, No. 3, 1971, pp. 275–285.
- [3] Ju, Y., Macheret, S., Miles, R., and Sullivan, D., "Numerical study of the effect of microwave discharge on the premixed methane-air flame," 40th AIAA/ASME/SAE/ASEE Joint Propulsion Conference and Exhibit, 2004, p. 3707.
- [4] Stockman, E. S., Zaidi, S. H., Miles, R. B., Carter, C. D., and Ryan, M. D., "Measurements of combustion properties in a microwave enhanced flame," *Combustion and Flame*, Vol. 156, No. 7, 2009, pp. 1453–1461.
- [5] Michael, J. B., Chng, T. L., and Miles, R. B., "Sustained propagation of ultra-lean methane/air flames with pulsed microwave energy deposition," *Combustion and Flame*, Vol. 160, No. 4, 2013, pp. 796–807.
- [6] Chen, B.-S., Garner, A. L., and Bane, S. P., "Simulation of flame speed enhancement of a hydrocarbon flame with a microwave field," *Combustion and Flame*, Vol. 207, 2019, pp. 250–264.
- [7] Adamovich, I. V., Macheret, S. O., Rich, J. W., and Treanor, C. E., "Vibrational relaxation and dissociation behind shock waves. Part 1-Kinetic rate models." *AIAA journal*, Vol. 33, No. 6, 1995, pp. 1064–1069.
- [8] Park, C., Howe, J. T., Jaffe, R. L., and Candler, G. V., "Review of chemical-kinetic problems of future NASA missions. II-Mars entries," *Journal of Thermophysics and Heat transfer*, Vol. 8, No. 1, 1994, pp. 9–23.
- [9] Armenise, I., Capitelli, M., and Gorse, C., "Nitrogen nonequilibrium vibrational distributions and non-Arrhenius dissociation constants in hypersonic boundary layers," *Journal of thermophysics and heat transfer*, Vol. 12, No. 1, 1998, pp. 45–51.
- [10] Ju, Y., and Sun, W., "Plasma assisted combustion: Dynamics and chemistry," Progress in Energy and Combustion Science, Vol. 48, 2015, pp. 21–83.
- [11] Winters, C., Hung, Y.-C., Jans, E., Eckert, Z., Frederickson, K., Adamovich, I. V., and Popov, N., "OH radical kinetics in hydrogen-air mixtures at the conditions of strong vibrational nonequilibrium," *Journal of Physics D: Applied Physics*, Vol. 50, No. 50, 2017, p. 505203.
- [12] Cutler, A. D., Cantu, L. M., Gallo, E. C., Baurle, R., Danehy, P. M., Rockwell, R., Goyne, C., and McDaniel, J., "Nonequilibrium supersonic freestream studied using coherent anti-Stokes Raman spectroscopy," AIAA Journal, Vol. 53, No. 9, 2015, pp. 2762–2770.
- [13] Messina, D., Attal-Tretout, B., and Grisch, F., "Study of a non-equilibrium pulsed nanosecond discharge at atmospheric pressure using coherent anti-Stokes Raman scattering," *Proceedings of the combustion institute*, Vol. 31, No. 1, 2007, pp. 825–832.
- [14] Roy, S., Meyer, T. R., Lucht, R. P., Afzelius, M., Bengtsson, P.-E., and Gord, J. R., "Dual-pump dual-broadband coherent anti-Stokes Raman scattering in reacting flows," *Optics letters*, Vol. 29, No. 16, 2004, pp. 1843–1845.
- [15] Lucht, R. P., "Three-laser coherent anti-Stokes Raman scattering measurements of two species," *Optics letters*, Vol. 12, No. 2, 1987, pp. 78–80.
- [16] Eckbreth, A. C., and Anderson, T. J., "Dual broadband CARS for simultaneous, multiple species measurements," *Applied optics*, Vol. 24, No. 16, 1985, pp. 2731–2736.
- [17] Montello, A., Nishihara, M., Rich, J., Adamovich, I., and Lempert, W., "Nitrogen vibrational population measurements in the plenum of a hypersonic wind tunnel," *AIAA journal*, Vol. 50, No. 6, 2012, pp. 1367–1376.
- [18] Filimonov, S., and Borysow, J., "Vibrational and rotational excitation within the X 1 Σ state of N2 during the pulsed electric discharge and in the afterglow," *Journal of Physics D: Applied Physics*, Vol. 40, No. 9, 2007, p. 2810.

- [19] Devyatov, A., Dolenko, S., Rakhimov, A., Rakhimova, T., Roi, N., and Suetin, N., "Investigation of kinetic processes in molecular nitrogen by the CARS method," Sov. Phys.—JETP, Vol. 63, 1986, pp. 246–50.
- [20] Dedic, C. E., and Michael, J. B., "Evaluation of vibrational excitation in a microwave plasma enhanced flame using hybrid fs/ps CARS," 2018 AIAA Aerospace Sciences Meeting, 2018, p. 1025.
- [21] Dedic, C. E., and Michael, J. B., "Thermalization dynamics in a pulsed microwave plasma-enhanced laminar flame," Combustion and Flame, Vol. 227, 2021, pp. 322–334.
- [22] Capitelli, M., Ferreira, C. M., Gordiets, B. F., and Osipov, A. I., Plasma kinetics in atmospheric gases, Vol. 31, Springer Science & Business Media, 2013.
- [23] Tsuchiya, S., "Emission and Absorption of the Sodium D-Line behind a Shock Wave in Argon, Nitrogen-and Carbon Monoxide-Argon Mixtures Containing a Trace of Sodium Vapor," *Bulletin of the Chemical Society of Japan*, Vol. 37, No. 6, 1964, pp. 828–842.
- [24] Millikan, R. C., and White, D. R., "Vibrational energy exchange between N2 and CO. The vibrational relaxation of nitrogen," The Journal of Chemical Physics, Vol. 39, No. 1, 1963, pp. 98–101.
- [25] Hurle, I., "Line-Reversal Studies of the Sodium Excitation Process Behind Shock Waves in N2," *The Journal of Chemical Physics*, Vol. 41, No. 12, 1964, pp. 3911–3920.
- [26] Frederickson, K., Leonov, S., Nishihara, M., Ivanov, E., Adamovich, I. V., Lempert, W. R., and Rich, J. W., "Energy conversion in high enthalpy flows and non-equilibrium plasmas," *Progress in Aerospace Sciences*, Vol. 72, 2015, pp. 49–65.
- [27] Tiwari, N., Bhandari, S., and Ghorui, S., "Stability and structures in atmospheric pressure DC non-transferred arc plasma jets of argon, nitrogen, and air," *Physics of Plasmas*, Vol. 25, No. 7, 2018, p. 072103.
- [28] Taylor, B., Kessler, D., Gamezo, V., and Oran, E., "Numerical simulations of hydrogen detonations with detailed chemical kinetics," *Proceedings of the combustion Institute*, Vol. 34, No. 2, 2013, pp. 2009–2016.
- [29] Nilsson, E., Hurtig, T., Ehn, A., and Fureby, C., "A setup for studies of laminar flame under microwave irradiation," *Review of Scientific Instruments*, Vol. 90, No. 11, 2019, p. 113502.
- [30] Miller, J. D., Slipchenko, M. N., Meyer, T. R., Stauffer, H. U., and Gord, J. R., "Hybrid femtosecond/picosecond coherent anti-Stokes Raman scattering for high-speed gas-phase thermometry," *Optics letters*, Vol. 35, No. 14, 2010, pp. 2430–2432.
- [31] Prince, B. D., Chakraborty, A., Prince, B. M., and Stauffer, H. U., "Development of simultaneous frequency-and time-resolved coherent anti-Stokes Raman scattering for ultrafast detection of molecular Raman spectra," *The Journal of chemical physics*, Vol. 125, No. 4, 2006, p. 044502.
- [32] Hancock, R. D., Bertagnolli, K. E., and Lucht, R. P., "Nitrogen and hydrogen CARS temperature measurements in a hydrogen/air flame using a near-adiabatic flat-flame burner," *Combustion and Flame*, Vol. 109, No. 3, 1997, pp. 323–331. https://doi.org/10.1016/S0010-2180(96)00191-5.
- [33] Dedic, C. E., "Hybrid fs/ps coherent anti-Stokes Raman scattering for multiparameter measurements of combustion and nonequilibrium," Ph.D. thesis, 2017.
- [34] Miller, J. D., Roy, S., Slipchenko, M. N., Gord, J. R., and Meyer, T. R., "rotational hybrid femtosecond / picosecond coherent anti-Stokes Raman scattering," Optics express, Vol. 19, No. 16, 2011, pp. 15627–15640.
- [35] Kearney, S. P., and Scoglietti, D. J., "Hybrid femtosecond/picosecond rotational coherent anti-Stokes Raman scattering at flame temperatures using a second-harmonic bandwidth-compressed probe," *Optics Letters*, Vol. 38, No. 6, 2013, pp. 833–835.
- [36] Storn, R., and Price, K., "Differential Evolution A Simple and Efficient Heuristic for global Optimization over Continuous Spaces," *Journal of Global Optimization*, Vol. 11, No. 4, 1997, p. 341–359. https://doi.org/10.1023/a:1008202821328.
- [37] Burkhart, S., "Coaxial E-field probe for high-power microwave measurement (short papers)," *IEEE transactions on microwave theory and techniques*, Vol. 33, No. 3, 1985, pp. 262–265.
- [38] Goodwin, D. G., Speth, R. L., Moffat, H. K., and Weber, B. W., "Cantera: An Object-oriented Software Toolkit for Chemical Kinetics, Thermodynamics, and Transport Processes," https://www.cantera.org, 2021. https://doi.org/10.5281/zenodo.4527812, version 2.5.1.
- [39] Smith, G. P., "GRI-Mech 3.0," http://www. me. berkley. edu/gri_mech/, 1999.

- [40] Hagelaar, G., and Pitchford, L. C., "Solving the Boltzmann equation to obtain electron transport coefficients and rate coefficients for fluid models," *Plasma Sources Science and Technology*, Vol. 14, No. 4, 2005, p. 722.
- [41] Pitchford, L. C., Alves, L. L., Bartschat, K., Biagi, S. F., Bordage, M.-C., Bray, I., Brion, C. E., Brunger, M. J., Campbell, L., Chachereau, A., et al., "Lxcat: An open-access, web-based platform for data needed for modeling low temperature plasmas," *Plasma Processes and Polymers*, Vol. 14, No. 1-2, 2017, p. 1600098.
- [42] "Hayashi database,", retrieved December on 4,2020. URL www.lxcat.net.
- [43] "Morgan database,", retrieved December on 4,2020. URL www.lxcat.net.
- [44] "Phelps database,", retrieved December on 4,2020. URL www.lxcat.net.
- [45] "SIGLO database,", retrieved December on 4,2020. URL www.lxcat.net.
- [46] Millikan, R. C., and White, D. R., "Systematics of vibrational relaxation," The Journal of chemical physics, Vol. 39, No. 12, 1963, pp. 3209–3213.
- [47] Michael, J., Dogariu, A., Shneider, M., and Miles, R., "Subcritical microwave coupling to femtosecond and picosecond laser ionization for localized, multipoint ignition of methane/air mixtures," *Journal of Applied Physics*, Vol. 108, No. 9, 2010, p. 093308.
- [48] Thompson, R. J., and Dedic, C. E., "Hybrid fs/ps CARS for quantifying CO and CO2," AIAA SCITECH 2022 Forum, 2022, p. 0893.